ELSEVIER

Contents lists available at ScienceDirect

Powder Technology

journal homepage: www.elsevier.com/locate/powtec



Assessing predictability of packing porosity and bulk density enhancements after dry coating of pharmaceutical powders



Kuriakose Kunnath, Liang Chen ¹, Kai Zheng, Rajesh N. Davé *

New Jersey Center for Engineered Particulates, New Jersey Institute of Technology, Newark, NJ 07102, USA

ARTICLE INFO

Article history: Received 27 March 2020 Received in revised form 16 September 2020 Accepted 18 September 2020 Available online 22 September 2020

Keywords:
Powder bed porosity prediction
Dry coating
Granular bond number
Porosity reduction
Particle surface roughness

ABSTRACT

Ability to predict the porosity, and its reduction after nano-silica dry coating, based on the Bond number and cohesion force estimated via multi-asperity contact model was examined for twenty different pharmaceutical powders. A new model for first order estimates of bulk density improvements after dry coating was found to be reasonably predictive despite variations in size ($10-225\,\mu\text{m}$), particle size distribution, aspect ratios (1-3.5), material density, and dispersive surface energy. For the porosity prediction model based on Bond numbers, Microcrystalline Cellulose (MCC) excipients were outliers, regardless of size ($20-200\,\mu\text{m}$). Analysis of their shape, surface morphology and specific surface areas (SSA), indicated that compared to other powders, MCCs had the highest SSA compared to equivalent spheres and high macro-roughness, while having high aspect ratios. This unique characteristic made them effectively more cohesive leading to their poor packing independent of their size, which is in line with previous simulations.

© 2020 Elsevier B.V. All rights reserved.

1. Introduction

Packing of dry powders is one of the important critical quality attributes (CQAs) that impact pharmaceutical processing and product properties, especially for direct compression tablet manufacturing [1–6]. Powder packing is also an important indicator of powder flow, and powders that pack well also flow well and vice a versa, thus packing is clearly a key CQA [7]. Previous studies have discussed the importance of bulk powder packing on various unit operations such as compaction [1–3] and feeding [1–4]. There also exist suggested guidelines in terms of acceptable packing density and flowability that may facilitate highspeed direct compression tableting, indicating the importance of powder and blend packing [8]. Consequently, formulators spend much time in developing pharmaceutical formulations with adequate bulk powder packing. Therefore, it would be beneficial to have mechanistic methodologies [9-12] and not just data-driven approaches [13] to be able to predict and manage bulk powder behavior, such as packing for individual powders as well as their blends, so that the probability of manufacturing failures can be reduced. In addition, when packing or bulk density of powders or their blends is marginal, it is advisable to consider reducing the failure probability by dry coating of APIs [5,10–12,14–22] or excipients [23,24], which helps improve powder packing. Dry coating involves surface modification of host particles by coating them with nano-sized guests, which reduces surface roughness of host particles and reduces the interparticle cohesion, leading to enhanced bulk density and flowability [25,26]. Consequently, this paper examines prediction of packing behavior of pharmaceutical powders with or without dry coating.

For non-cohesive, monodisperse, spherical powders, their random loose packing density is well-known, and it does not depend on the particle size as long as the size is large enough [27]. However, for predicting packing or porosity of well-flowing spherical powders with nonuniform size distributions, empirical relationships that account for particle size distribution need to be derived, see extensive work by Yu and Standish [28,29]. Such models also allow predicting porosity of binary and ternary mixtures or blends [27–29]. However, as particles get smaller, the powder cohesion becomes increasingly important, and van der Waals (vdW), electrostatic, or capillary forces are considered dominant, posing additional challenges to predicting their bulk behavior [6,9].

Yu et al. demonstrated that for fine glass spheres, the effect of interparticle cohesion is more influential compared to that for coarse glass spheres [9]. Generally, porosity is inversely related to the particle size of glass spheres. However, theoretically calculated interparticle force also increases with particle size [9]. To account for this, Yu et al. normalized the interparticle force with the weight of a particle, and coined this the "force ratio", allowing them to introduce mechanistic aspects in to a semi-empirical model [9]. They demonstrated a relationship between the force ratio and porosity for ideal glass spheres with relatively low cohesion [9]. It is noted that the force ratio is essentially the same as what is popularly known as the granular Bond number [9,30]. Capece

^{*} Corresponding author at: Chemical and Materials Engineering, New Jersey Center for Engineered Particulates, New Jersey Institute of Technology, Newark, NJ 07102, USA. E-mail address: dave@njit.edu (R.N. Davé).

¹Current address: Product and Technical Development, Biogen, 225 Binney St., Cambridge, MA 02142, United States of America.

K. Kunnath, L. Chen, K. Zheng et al. Powder Technology 377 (2021) 709–722

et al. investigated the use of the Bond number to predict the porosity of commonly used pharmaceutical powders with varying particle sizes and shapes, which deviated from spherical [11]. Capece et al. incorporated a multi-asperity contact model [25] to better estimate the particle adhesion forces and demonstrated the improved model's ability to consider the effects of dry powder processing [11], which would not have been possible with purely empirical models. Additionally, in their work, powders were dry coated with varying types and sizes of nanosized guest particles to vary the interparticle cohesion yet maintain the original particle size of various powders [11]. They demonstrated the applicability of the contact models in conjunction with the Bond number models to account for such surface modification via dry coating, and attributed this ability to the incorporation of particle scale physics in Bond number models [11]. Capece et al. also discussed the problem of estimating the particle surface asperity that is important in estimating interparticle cohesion, and also discussed that for dry coated powders, that problem is trivially solved, and that dry coating also leads to significant reduction in powder porosity [13].

Notwithstanding the major advances represented by these mechanistic models [9,11], there are several outstanding issues that need to be addressed. First, these models assume spherical shape and implicitly assume monodisperse particle sizes. Interestingly, Capece et al. included nine realistic industrial powders, of which five were rather cohesive, that had neither spherical shapes nor monodisperse sizes, yet the predictive capability was remarkable [11]. Second, these models require good estimation of the particle cohesion for estimating the Bond number. While the Chen model [25] worked well for all the powders used by Capece et al. [11] even when it assumes spherical powders and uniform asperity sizes and their distributions. Third, estimating the Bond number requires the use of a representative average particle size of the powder sample for which there are various averaging choices, including a novel idea of geometric averaging that uses particle surface area as weights in averaging, allowing for potentially capturing the effect of a wide size distribution or even blends of different powders [10,12]. Some of these ideas could be applied for a wider variety of pharmaceutical powders that may pose additional challenges to the Capece et al. model [11]. For example, Hoffmann et al. have stated that in general, it is difficult to predict the packing of powders which contain flake-like or rod shaped particles [31]. Through simulations using discrete element method (DEM), Deng and Davé investigated packing behavior of cohesive, high aspect ratios particles [32]. It was found that the combined effect of higher aspect ratios and higher cohesion contribute to poorer packing, which was relatively independent of particle size [32]. Other factors such as intraparticle porosity have also been reported to affect powder packing. As industrial powders tend to deviate greatly from ideal assumptions of spherical, smooth, solid particles, future model enhancements would need to account for expected deviations. In addition, previous work did not consider direct model for predicting the extent of porosity reduction or bulk density enhancement after dry coating. For pharmaceutical practitioners, having such capability would be beneficial even if the prediction provides only first order, conservative estimates which would help justify further investigation.

In this paper, the purpose is to assess predictability of packing porosity as well as its bulk density reduction enhancements after dry coating for a wider variety of pharmaceutical powders, with and without dry coating. Towards that goal, twenty different powder samples are considered that include many cohesive drug powders and excipients, including those with appreciable aspect ratios as well as surface roughness. First, the packing behavior of all these powders before and after dry coating and the extent of the enhancements after dry coating will be examined, along with the ability to predict such enhancements. For assessing the existing porosity prediction model, two enhancements [11] will be considered. First, the use of entire particle size distributions, as demonstrated in [10,12], will be considered with the hope to improve powder bed porosity prediction. Second, the usual assumption of 200 nm asperity size for particles, which is recommended as a good

approximation based on experimental work by Massimilla and Donsì [33], will be tested. As an alternate, the applicability of estimating the asperity size as a power function of the particle size will be examined [9,11]. In addition, for the cases that appear to be significant outliers for prediction, the asperity sizes that better allow porosity prediction will be back calculated to further examine the role of asperities.

2. Theory

The Bond number for a powder is defined as the ratio of interparticle force to the gravitational force acting on one particle [30]. This concept, which has been previously proven to be able to predict bulk scale properties, can be visualized in Fig. 1 and is computed using Eq. 1.

$$Bo_g = \frac{F_{ad}}{W_g} \tag{1}$$

Here, F_{ad} is the interparticle force exerted on one particle by another particle, and W_g is the gravitational force (particle weight). It is important to state the assumptions of this model, which are: (1) spherical mono-sized particles with no agglomeration, (2) uniform particle surface in terms of asperity size and surface energy, and (3) van der Waals forces are the dominant interparticle force for dry powders, thus electrostatic and capillary forces can be ignored. In the case where dry particle coating with nano-silica is implemented, additional assumptions include well-mixedness and no deformation of particles. The computation of the gravitational force (W_g) acting on one particle is straightforward, and is given in Eq. 2.

$$W_g = \frac{\pi}{6} D^3 \rho_p g \tag{2}$$

Continuing with the assumption of mono-sized spherical particles, the weight can be calculated as the product of volume, true density (ρ_p) , and acceleration due to gravity (g) of the particle. In Eq. 2, D is the particle size.

The computation of the interparticle force between two particles (F_{ad}) is a critical step and it needs to take into account surface roughness, and sparse or dense population of surface asperities or the presence of dry-coated nanoparticles [25]. For densely populated asperities, multiple-asperities of one particle can contact one asperity of another particle, for which Eq. 3 representing the multi-asperity model can be used, which assumes smooth spherical particles with small well-populated asperities on the surface [25].

$$F_{ad} = \frac{Ad}{8z_0^2} + \frac{AD}{24(2d+z_0)^2} \tag{3}$$

This model takes into consideration the particle size (D), the surface energy via Hamaker constant (A), the minimum separation distance

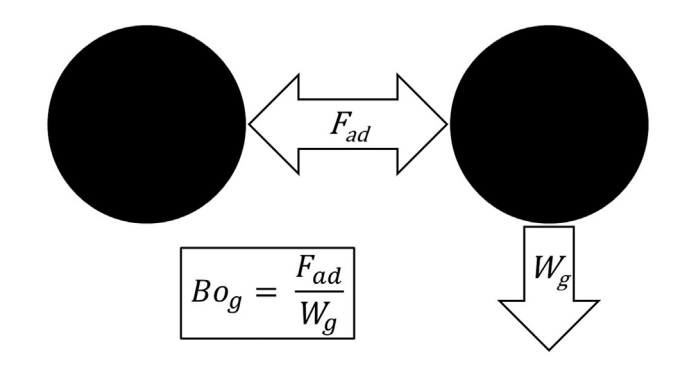


Fig. 1. Schematic of Bond number, which is the ratio of interparticle force (F_{ad}) to the weight of a particle (W_g) .

between two particles in contact (z_0) , and the surface asperity size of the particles, or the diameter of nanoparticles in case of dry coating (d). The minimum separation distance (z_0) is taken as 0.4 nm, and the Hamaker constant (A) can be calculated using Frenkel relation described in Eq. 4.

$$A = 24\pi D_0^2 \gamma_d \tag{4}$$

Here, γ_d is the dispersive surface energy of the powder and D_0 is the cut off distance, taken as 0.165 nm [34]. However, judicious selection of particle size (D) and the surface asperity size (d) is not straightforward, and will be further discussed in this subsection.

For sparsely coated particles, predominant contacts between two particles are guest-host type and account for the extent of surface area coverage (SAC), which will be discussed further in Section 3. In that case, the adhesion force is given by Eq. 5, where L_0 is the separation distance between two coated particles, given by Eq. 6 [25].

$$F_{ad} = \frac{Ad}{4z_0^2} + \frac{AD}{24(L_0)^2} \tag{5}$$

$$L_0 = \sqrt{(d+D)^2 - \frac{1.21}{SAC}d^2} - D \tag{6}$$

To calculate the interparticle force using Eqs. 3 or 5, various particle size descriptors can be used for the particle size value (D). Among these are median particle size (d_{50}) [6,9,11,25,26,35–37] and the Sauter mean diameter $(d_{3,2})$ [10,12], both of which can be attained via laser diffraction particle sizing. Although it is assumed that particles are spherical, in reality this is rarely the case for commonly used pharmaceutical powders. The Sauter mean diameter $(d_{3,2})$ is defined as the diameter of a sphere which has the same surface area to volume ratio as an irregular, non-spherical particle. In particle technology, the $(d_{3,2})$ is often used to account for particle shape irregularities, which can lead to increased surface area. Increases in surface area can increase interparticle cohesion, and using median particle size (d_{50}) may not be able to account for this. In such cases, it may be more appropriate to use the Sauter mean diameter $(d_{3,2})$, instead of the median particle size (d_{50}) .

Additionally, a size class dependent Bond number can be calculated for a powder sample. It was previously mentioned that mono-sized spherical particles are a major assumption for Bond number approximations. However, recent studies have developed an approach to incorporate particle size distribution into calculations for interparticle force and particle weight, which allows for incorporation of interactions between particles of different sizes [10,12]. Eq. 7 describes the size class dependent Bond number ($Bo_{g,mix}$), and Eq. 8 describes the fractional surface area weighting function (w_{ij}), which is based on the theoretical fractional surface area (f_{SA}) for each size class.

$$Bo_{g,mix} = \left(\sum_{i=1}^{K} \sum_{j=1}^{K} \frac{w_{ij}}{Bo_{g,ij}}\right)^{-1}$$
 (7)

$$w_{ij} = f_{SA,i} f_{SA,j} \tag{8}$$

For interactions between particles of different sizes, the harmonic mean of the two particle sizes is used for calculation, as described in Eq. 9.

$$D_{ij} = \frac{2D_i D_j}{D_i + D_j} \tag{9}$$

Other values such as dispersive surface energy (γ_d) , Hamaker constant (A), surface asperity size (d), and particle density (ρ_p) are assumed to be constant for particles of the same material, but in different size classes. In previous studies, surface asperity size (d) is often taken as a constant value (200 nm), based on experimental results by Massimilla

and Donsì [25,33]. Alternatively, several studies have demonstrated estimating the asperity size (d) as a function of the particle size via an empirical relationship, which is displayed in Eq. 10 [9,11].

$$d = \alpha D^{\beta} \tag{10}$$

Here, α and β are fitted constants with values of 4×10^{-4} and 0.6 respectively [11]. Both of these approaches are considered adequate for dry powders, and several studies have demonstrated their use in Bond number based bulk property prediction [9,11,12]. Additionally, it is important to consider cases where surface asperity size (d) may change, such as dry coating with nano-silica. For such cases, where nano-silica particles adhere to the particle surface, the size of the nano-silica can be taken as the new surface asperity size (d) [9].

3. Materials and methods

3.1. Materials

A total of 20 commonly used pharmaceutical powders were used in this study, along with one glidant to be used for dry coating. Among these are 7 Active Pharmaceutical Ingredients (APIs), which are listed in Tables 1, and 13 excipients listed in Table 2. These tables include relevant information regarding the powders, such as manufacturer, median particle size (d_{50}) , Sauter mean diameter $(d_{3,2})$, particle (true) density (ρ_p) , and dispersive surface energy (γ_d) . Additionally, nanosilica (glidant) was used for dry coating applications. In this study, hydrophobic R972P pharmaceutical grade nano-silica was used as the glidant, which was donated by Evonik, USA. R972P nano-silica has a nominal particle size (d) of 20 nm, with a particle density (ρ_{σ}) of 2650 kg/m³, and a surface energy (γ_d) of 36.40 mJ/m², which was measured experimentally by Chen et al. [24]. Since R972P is used for dry coating, it will attach onto the surface of pharmaceutical powders, and is assumed to become the new asperity size, hence the notation "d" (surface asperity size) is used for R972P particle size instead of "D" (particle size).

3.2. Methods

3.2.1. Dry coating via LabRAM

Dry coating of pharmaceutical powders was carried out in a high-intensity vibratory mixer, called the Resonance Acoustic Mixer (LabRAM, Resodyn Corporation, USA). The pharmaceutical powder (50 g) and a certain amount of glidant (R972P), were put in a cylindrical plastic jar (9.5 cm height, 8 cm inner diameter), and clamped into the LabRAM, where it was shaken at high intensity (75 G's acceleration) for 5 min at a frequency of 60 Hz. Determination of glidant amount, reported in supplementary materials (Table S1), was based on theoretical 100% surface area coverage (SAC) calculated using Eqs. 11–13 [25].

$$Wt\% = \frac{nd^3\rho_g}{D^3\rho_p + nd^3\rho_g} *100\%$$
 (11)

$$n = \frac{2\sqrt{3}\pi D^2}{9R_c} \tag{12}$$

$$R_c^2 = \left(\frac{D+d}{2}\right)^2 - \left(\frac{D+L_0}{2}\right)^2 \tag{13}$$

In these Equations, n is the number of guest particles it takes to cover the surface of a host particle, d is the guest particle size, ρ_g is the guest particle density, D is the host particle size, ρ_p is the host particle density, R_c is the contact radius, L_0 is the separation distance between two host particles (Eq. 6), and SAC is the theoretical surface area coverage. Further details of theoretical 100% SAC weight percentage calculations

Table 1The active pharmaceutical ingredient (API) materials used in this study, along with their manufacturers, particle size data, true density, and dispersive surface energy. Asterisk markers signify powders which were also used in Capece et al. [11].

Material	Manufacturer	Median particle size, d_{50} (μm)	Sauter mean diameter, $d_{3,2}$ (μm)	True density, ρ_p (kg/m ³)	Dispersive surface energy, $\gamma_d \ (mJ/m^2)$
*Micronized Acetaminophen (mAPAP)	Changshu Huagang Pharmaceutical Co., Ltd. China	7.31	4.82	1290 ^a	46.38
*Coarse Acetaminophen (cAPAP)	Mallinckrodt, Inc., USA	23.25	17.54	1290 ^a	40.86
*Ibuprofen 50 (IBU50)	BASF, USA	52.76	32.20	1120 ^a	38.92
*Ascorbic Acid (AA)	Ruger, USA	224.28	123.35	1650 ^a	41.00
Fenofibrate (FNB)	Jai Radhe Sales	6.82	4.52	1263	39.50
Griseofulvin (GF)	Lecto Medical, USA	10.56	6.37	1430	39.70
Itraconazole (ITZ)	Jai Radhe Sales	10.03	5.26	1365	36.40

^{*} Powders also used in Capece et al. [11] and plotted in Fig. 5.

can be found in Chen et al. [25]. While mixing in LabRAM, nano-silica glidant (guest) agglomerates attach to the host, are broken up into primary particles, and get evenly distributed onto the surface of host particles (pharmaceutical powders). Previous studies have proven and discussed how this method can reduce the interparticle cohesion of powders, while maintaining particle size [5,11,15–17,20–26].

3.2.2. Particle size analysis

All particle size measurements were performed using a RODOS/HELOS dry dispersion laser diffraction particle sizer (Sympatec, USA). Dispersion pressure was set to 0.5 bar, and volume based particle size statistics are reported in Tables 1 and 2. The Fraunhofer Enhanced Evaluation (FREE) and Mie Extended Evaluation (MIEE) theories of light scattering were used to determine particle sizes by the HELOS unit. PSD analyses were performed 3 times and average values are reported. Due to excellent repeatability, the standard deviations are not reported. Additionally, it was assumed that after dry coating, the PSD of the powder does not change or is negligible, as was demonstrated in previous literature [21,24].

3.2.3. Particle (true) density analysis

Particle (true) density $(\rho_{\rm g})$ of each powder was analyzed via Pycnomenter (NOVA 3200, Quantachrome Instruments, Boynton Beach, FL, USA) with Helium gas. The experiment was repeated 5 times, and average values are reported.

3.2.4. Surface energy analysis

Dispersive surface energy (γ_d) of each powder was determined via inverse gas chromatography, using a Surface Energy Analyzer (SEA-

iGC, Surface Measurement Systems Ltd., Middlesex, UK). A known amount of powder sample was poured in cylindrical silanized glass columns (4 mm inner diameter, 30 cm length), bookended with silanized glass wool, and tapped for 5 min to attain adequate powder packing. Initially, Helium was used to condition the powders, and remove impurities and moisture. The conditioning step was carried out at 303 K column temperature, 453 K injector and detector temperature, 0% relative humidity, and 10 mL/min Helium flow rate for 120 min. Afterwards, gas probes (Hexane, Heptane, Octane, Nonane, and Decane) were injected into the column, and retention times were obtained for each probe separately. Lifshitz-van der Waals (LW) dispersive surface energy was attained via Schultz method [38], and all reported data are for infinite dilution (3% surface coverage of sample with gas probes). Further details of the SEA-iGC operation can be found in [19].

3.2.5. Scanning electron microscopy

A Field Emission Scanning Electron Microscope (SEM, JSM 7900F, Jeol Ltd., Peabody, MA, USA) was used to study morphology and particle surfaces of powders. Prior to SEM imaging, samples were sputter-coated with Carbon (Q150T, Quorum Technologies Ltd., Laughton, East Sussex, England) to enhance their conductivity.

3.2.6. Surface area analysis

Specific surface area (SSA) of each powder was measured via Brunauer-Emmett-Teller (BET) theory using a Quantachome ASiQWin, with Autosorb iQ software for analysis. A known amount of powder sample was loaded into a 6 mm ID tube with glass bulb at the bottom. Degassing was carried out under vacuum and the degassing temperature and time was varied for each powder sample, based on their

Table 2The excipient materials used in this study, along with their manufacturers, particle size data, true density, and dispersive surface energy. Asterisk markers signify powders which were also used in Capece et al. [11].

Material	Manufacturer	Median Particle Size, d ₅₀ (μm)	Sauter Mean Diameter, d _{3,2} (μm)	True Density, ρ_p (kg/m ³)	Dispersive Surface Energy, γ_d (mJ/m ²)
*Cornstarch (CS)	Argo	14.37	15.00	1444	32.34
Granulac 200 (Gran200)	Mutchler Inc., USA	27.94	10.27	1528	34.37
*Granulac 230 (Gran230)		21.98	7.36	1546	34.37
Lactose 120 (Lac120)		93.87	38.93	1504	37.46
*Sorbolac 400 (Sorb400)		8.69	4.29	1520	43.44
Pharmatose 350 (Pharm350)	DFE Pharma, USA	28.25	26.00	1540	41.82
Pharmatose 450 (Pharm450)		19.19	17.00	1543	44.69
Pharmatose DCL11 (DCL11)		115.37	85.18	1543	39.48
Avicel 101 (Av101)	FMC Biopolymer	64.24	42.94	1562 ^a	42.33 ^a
Avicel 102 (Av102)		116.59	65.97	1563 ^a	56.05 ^a
Avicel 105 (Av105)		18.97	10.84	1559 ^a	47.80 ^a
Avicel 200 (Av200)		185.89	100.43	1562 ^a	47.11 ^a
Avicel 301 (Av301)		64.20	39.84	1508	47.66

^{*} Powders also used in Capece et al. [11] and plotted in Fig. 5.

^a Data attained from Capece et al. [11].

^a Data attained from Capece et al. [10].

K. Kunnath, L. Chen, K. Zheng et al. Powder Technology 377 (2021) 709–722

melting points. Afterwards, an 11-point BET adsorption analysis (P/ $P_o = 0.05-0.3$) was conducted using Nitrogen gas at 77 K. SSA values were calculated from adsorption isotherms which have linear R^2 values above 0.9975 and positive C constants, as this will ensure the exclusion of possible internal pore area in SSA calculation [39].

3.2.7. Bulk density analysis via FT4 Powder Rheometer

An FT4 Powder Rheometer (Freeman Technology Ltd., UK) was used to measure bulk densities of powders. First, powder was loosely filled into a 25 mm \times 25 mL cylindrical vessel, and conditioned using a twisted blade. This conditioning step is designed to remove excess air, erase any previous consolidation effects, and create a uniform powder bed to perform the bulk density experiment. After conditioning, excess powder is removed by splitting the vessel to assure only 25 mL volume of the powder bed is remaining. At this point, the mass of the 25 mL volume of powder is measured to attain the ratio of powder mass to volume, i.e. bulk density. Since excellent repeatability was attained for samples after 3 repetitions, only the average values are reported in this study. The porosity (ε) of the powder bed is then calculated using Eq. 14, where ρ_b is the bulk density and ρ_p is the particle (true) density.

$$\varepsilon = 1 - \frac{\rho_b}{\rho_p} \tag{14}$$

4. Results and discussion

4.1. Experimental results

The most important factor affecting particle packing is particle size. Generally, as particle size increases, particle packing improves [11], i.e. bulk density increases, up until a certain point. Fig. 2a displays the experimental bulk density results of all as received (uncoated) powders, plotted against their median particle size (d_{50}). In this plot, the trend of increasing particle packing vs particle size holds true for almost all powders (solid markers), except in the case of Avicel powders (circle markers), which have similar bulk densities regardless of particle size. Such data is somewhat unexpected and has not been explicitly reported in previous literature. In this study, dry coating with hydrophobic R972P nano-silica was implemented, and bulk density results after dry coating are presented in Fig. 2b as a function of median particle size. As was the case in previous literature, results demonstrate increased particle packing (i.e. higher bulk density) after dry coating for all powders, and such results can be attributed to the ability of dry coating with nanoparticles to lower interparticle forces [5,11,15-20,22,24-26,40]. Additionally, the general trend of increasing bulk density vs particle size stays true for most powders (solid markers) after dry coating. However, the Avicel (circle markers) bulk densities remain fairly constant although they have improved appreciably. Comparing Fig. 2a and b for all cases, although dry coating improves bulk density, the general trends of increasing bulk density as a function of particle size remains the same, with the Avicels being the major outliers. These results also suggest that the accurate prediction of bulk density using previous models [11] in case of Avicels may pose a challenge.

In order to assess the effectiveness of dry coating, percent improvements in bulk density was calculated based on values before and after dry coating. It is important to note that all measured percent improvement values were positive numbers, meaning dry coating improved particle packing for all powders. In Fig. 3a, the percent improvements of bulk density are plotted against the Bond numbers of the corresponding as received powders. When fitted with a power fit, this relationship produces an R² value of 0.4753 and may not be accurately predictive. Yet, such relationship is useful enough to provide a preview of what level of improvements can be expected after dry coating. Generally, higher bulk density percent improvement values are observed for higher Bond number powders which are more cohesive. Powders

having higher Bond number generally have lower initial bulk densities, therefore they require higher % improvements, which was observed in Fig. 3. After dry coating, the interparticle forces are reduced by orders of magnitude [11,25,26], allowing for more significant increases in particle packing (bulk density). In contrast, lower percent improvement values are observed for lower Bond number powders. This is somewhat expected because lower Bond numbers indicate less cohesive powders that have decreased influence of interparticle forces compared to gravitational forces, and hence they naturally have relatively good particle packing which is close to the minimum possible porosity value ($\epsilon=0.4$ for random loose packing). Therefore, it is very difficult to further increase the particle packing value as the influence of interparticle forces can't be reduced much further. Fortunately, for those powders, dry coating may not be necessary since they are not very cohesive.

It is noted that Fig. 3a includes the Avicels (circle markers), which were outliers in Fig. 2. However, they are not outliers in this case, indicating that dry coating is very effective also for such powders. In fact, they follow the trend of higher percent improvement of bulk density at higher Bond number values. Unfortunately, there are two outliers in the bottom right hand corner of Fig. 3a, whose Bond numbers are relatively high (>1000), yet their percent improvement values are below 25%. These powders are Griseofulvin (API) and Sorbolac 400 (lactose excipient). From experimental data, both of these powders are not outliers of any metric when comparing their values against other powders in Tables 1 and 2. Their particle size metrics (d_{50}, d_{32}) are on the lower end of the particle size ranges, but there are powders with lower particle sizes, which have adequate percent improvement in bulk density. For example, micronized Acetaminophen (mAPAP) and Fenofibrate (FNB) have median particle sizes (d_{50}) of 7.31 μ m and 6.82 μ m, respectively, but have high percent improvement in bulk density values of 71% and 90%, respectively. Similarly, the particle (true) density and dispersive surface energies of Griseofulvin and Sorbolac 400 powders are middle of the pack. However, these powders have exceptionally large SSA values. Griseofulvin has a SSA of 5.04 m²/g, and Sorbolac 400 has a SSA of 2.63 m²/g, both of which are higher than all the SSA values given in Table 3. A reason for their poor percent improvement value with respect of Bond number could be the effective low surface area coverage (SAC) of the particle surface with R972P nano-silica. Here, 100% SAC values were calculated using Eqs. 11–13 to determine the amount of R972P nano silica to use during dry coating (see supplementary material S1). It is likely that the amount used for Griseofulvin and Sorbolac 400 may be insufficient. Eqs. 11–13 assume spherical particles, and do not take into account varying surface area. A possible explanation for Griseofulvin and Sorbolac 400 being outliers is that they may need more R97P nano-silica to cover up their higher than expected particle surface area, and/or they may require longer processing time to adequately distribute and cover all of the increased particle surfaces. In a nutshell, these two powders are outliers which may require further formulation/process development for dry coating. Fig. 3b displays the same data as Fig. 3a, except Griseofulvin and Sorbolac 400 are removed. The same power fit was used to fit Fig. 3b, and produces a much better fit with an R^2 value approaching 0.7.

Eq. 15 is a new empirical model for predicting the improvement in powder bulk density after dry coating, based on the power fit in Fig. 3.

$$BD_{\Delta Bo} = BD_{\Delta 1} \sqrt[a]{Bo_g} \tag{15}$$

Here, $BD_{\Delta Bo}$ is the percent increase in the bulk density after dry coating, and $BD_{\Delta 1}$ is the percent improvement in bulk density if $Bo_g=1$. For the best fitting case of Fig. 3b, $BD_{\Delta 1}$ is 15% and the root constant, a is 5 in Eq. 15. Therefore, a minimum of 15% improvement in Bulk density is expected for powders having Bond numbers at or above one. The constant a has a value of 5, implying relatively weak function of Bond number. However, since Bond number is a highly non-linear function of particle size, bulk density is actually a strong function of the inverse of particle



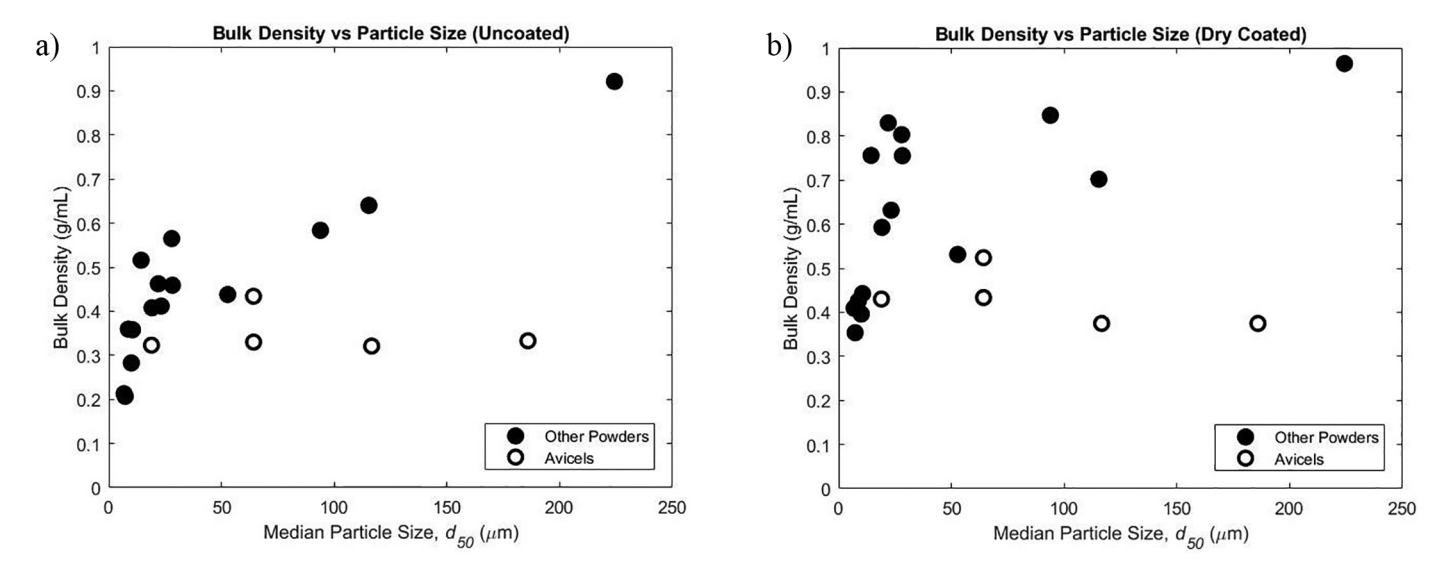


Fig. 2. Experimental bulk density values plotted against experimental median particle sizes (d_{50}) for (a) as received uncoated powders and (b) dry coated with R972P nano-silica powders. All dry coated powders were processed in LabRAM for 75Gs and 5 min with theoretical 100% SAC values of R972P, which are given in supplementary material S1. The trend of increasing bulk density as a function of median particle size does not hold true for most Avicel powders (circle markers).

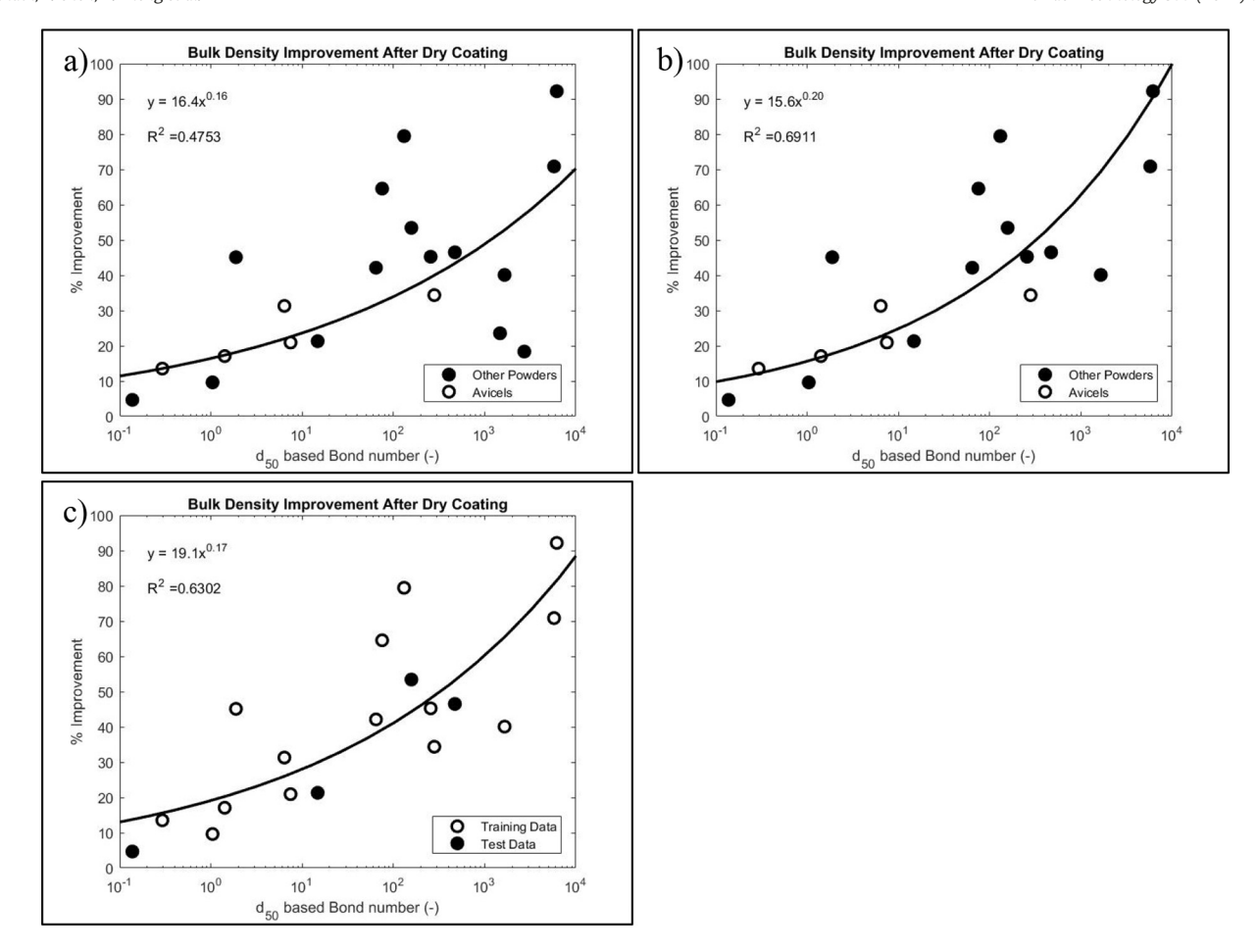


Fig. 3. Percent improvement in bulk density after dry coating vs as received median particle size based Bond number for (a) all powders and (b) all powders, excluding outliers Griseofulvin and Sorbolac 400. A power fit is used, producing a relatively good fit ($R^2 = 0.69$) without the outliers. A fit attained from using training data is displayed in (c), with circle markers being training data and solid markers being test data.

size. For the fine powders used in this study, Bond numbers can get very large (>1000), leading to significant percentage increases in bulk density, up to 90%. For a conservative estimate, Eq. 15 can use the fit in Fig. 3a, and then $BD_{\Delta 1}$ would be about 16% and the root constant, a would be about 6, implying the bulk density increase for finer powders would be as high as 70%. In summary, these Figures and Eq. 15 demonstrate that particle packing improvements via dry coating are a function of the Bond number of the uncoated powders, along with the adhesion models of Eqs. (3) and (5), and may be estimated a priori. This ability to estimate the expected enhancements after dry coating can guide

decision making regarding whether or not dry coating is necessary or would be beneficial. It is noted that since the data used for fitting the proposed empirical model is only from R972P silica coating, the model needs to be generalized to account for the type of the guest particles used. It is expected that the impact of the nano-sized guest type, i.e., its size and surface energy, would be captured through the constant, $BD_{\Delta 1}$. The predictive capability of Bond number based models is further considered in latter sections.

In order to verify that the power fit in Fig. 3B is robust and does not require use of the entire data set as the training set, a randomly selected

Table 3Bulk density, powder bed porosity, specific surface area, and back calculated asperity size values (to attain perfect porosity prediction) for all Avicel powders, and several others selected for comparison. The last 4 powders are APIs, for which accurate porosity prediction was attained both here and in previous publications.

	Median particle size, d_{50} (µm)	Sauter mean diameter, $d_{3,2}$ (µm)	Bulk density, ρ_b (g/mL)		Porosity, $\varepsilon\left(-\right)$		Specific surface area	Aspect ratio (-)	Correct back-calculated asperity size, d
			As received	Dry coated	As received	Dry coated	(m ² /g)		(nm)
Av 105	18.97	10.84	0.32	0.43	0.77	0.72	1.72	3.05	3630
Av 301	64.20	39.84	0.43	0.52	0.71	0.65	0.43	2.13	1.88*10 ⁴
Av 101	64.24	42.94	0.33	0.43	0.78	0.72	1.50	2.63	1.36*10 ⁵
Av 102	116.59	65.97	0.32	0.37	0.76	0.76	0.92	2.83	7.32*10 ⁵
Av 200	185.89	100.43	0.33	0.37	0.78	0.76	1.11	2.58	2.95*10 ⁶
mAPAP	7.31	4.82	0.21	0.35	0.84	0.73	0.77	3.47	681
cAPAP	23.25	17.54	0.41	0.63	0.68	0.51	0.39	2.64	418
IBU50	52.76	32.20	0.44	0.53	0.61	0.53	0.17	3.06	928
AA	224.28	123.35	0.92	0.96	0.44	0.42	0.08	1.34	84.2

Table 4Table of powders and data used to make Fig. 3B and C, along with % error for the respective plots. All powders except Griseofulvin and Sorbolac 400 were used here. The powders with asterisk markers (*) signify powders randomly chosen and reserved as test data, while all others were used as training data.

Material	<u>UC Bog</u> (-)	BD % Improvement	Fig. 3B <u>- %</u> Error	Fig. 3C <u>- %</u> Error
mAPAP	5761.1	70.85	-18.38	-9.72
*cAPAP	157.5	53.44	10.22	9.14
*Ibu50	14.8	21.31	-5.53	-8.59
*Ascorbic Acid	0.14	4.667	-5.80	-9.08
Fenofibrate	6169.7	92.18	1.70	10.68
Itraconazole	1653.3	40.09	-29.30	-25.39
*CS	471.4	46.51	-7.39	-6.64
Granulac 200	64.5	42.12	6.02	3.94
Granulac 230	130.9	79.45	37.81	36.49
Lactose 120	1.88	45.12	27.40	23.89
Pharmatose 350	75.3	64.56	27.31	25.37
Pharmatose 450	256.3	45.26	-2.41	-2.77
Pharmatose DCL11	1.04	9.630	-6.10	-9.61
Avicel 101	6.39	31.31	8.65	5.307
Avicel 102	1.41	17.08	0.35	-3.16
Avicel 105	280.9	34.38	-14.19	-14.40
Avicel 200	0.29	13.53	1.35	-2.05
Avicel 301	7.47	20.93	-2.46	-5.76

portion of data points was taken as the test data and the remaining points were used as the training data, with the results displayed in Fig. 3C. Here, 20% of the data points were randomly chosen as test

data, identified by asterisk markers in Table 4. The remaining 80% was used as training data to generate the fit in Fig. 3C, which has an $\rm R^2$ value of 0.6302. This fit using training data generates an $\rm R^2$ only slightly below the $\rm R^2$ value in Fig. 3B, implying prediction was approximately the same. Additionally, Table 4 compares % error values from the fits in Fig. 3B and C, which demonstrate that the use of training data does not have any adverse effect on the fit of Eq. 15. These results imply simply fitting the data points, as done in Fig. 3B, is fairly robust although as explained above, should be only used as a first order estimate of the expected enhancement.

4.2. Porosity vs bond number

After measuring bulk density (ρ_b) using the FT4 Powder Rheometer, Eq. 14 was used to calculate powder bed porosity (ε) of pharmaceutical powders. Fig. 4 displays the results of powder bed porosity (ε) plotted against the theoretically calculated Bond number. Markers represent experimental data points and the solid line is the Bond number based porosity (ε) prediction using Eqs. 1,3–9,16.

$$\varepsilon = \varepsilon_0 + (1 - \varepsilon_0) \exp\left(-mBo_g^{-n}\right) \tag{16}$$

In Eq. 16, porosity (ε) is predicted using the Bond number (Bo_g), and the values for constants ε_0 , m and n are 0.44, 3.09 and 0.224 respectively, which are from literature [11]. Fig. 4a was generated using median particle size (d_{50}) based Bond number, Fig. 4b using Sauter mean diameter ($d_{3,2}$) based Bond number, and Fig. 4c using size class dependent Bond

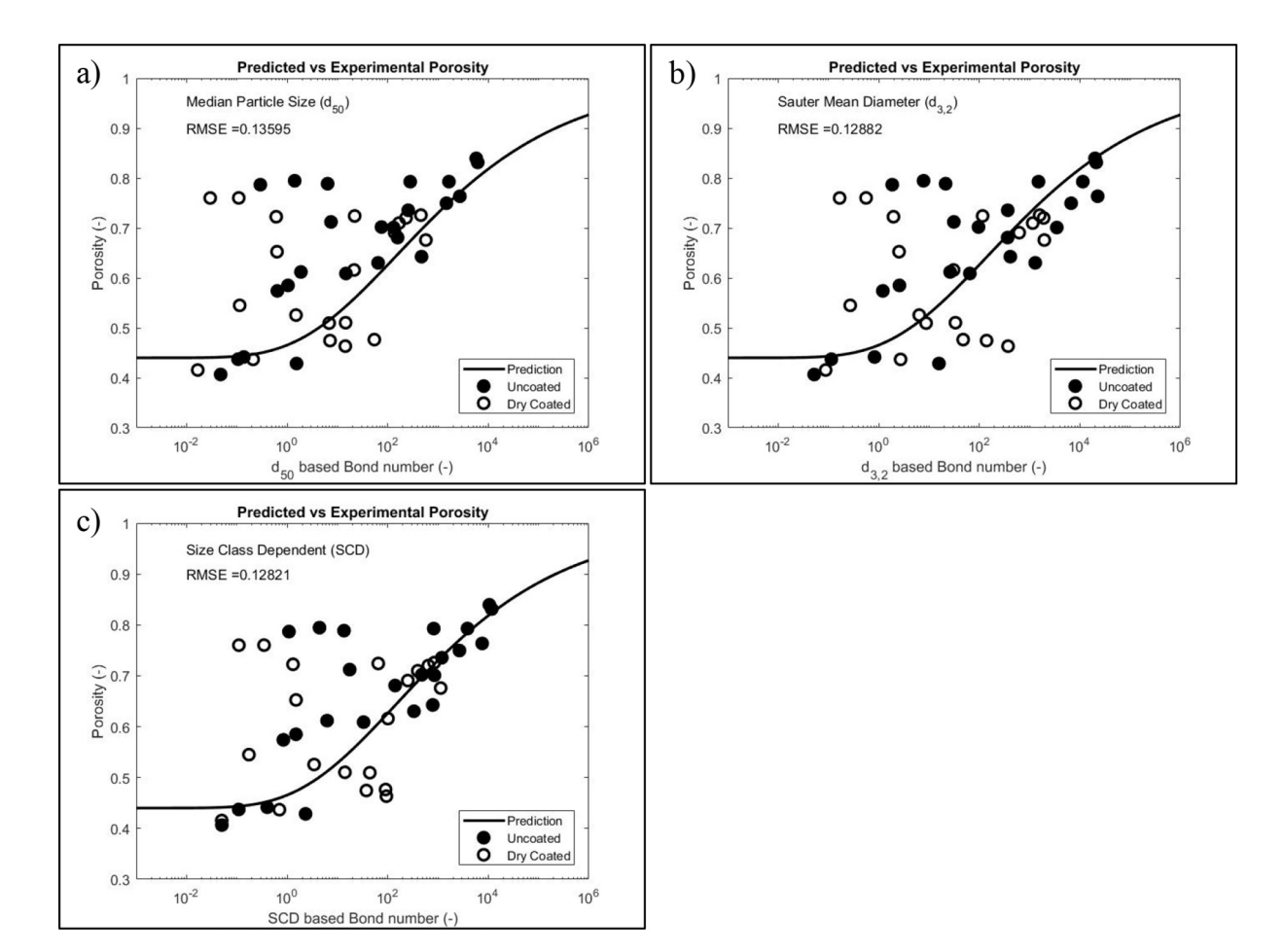


Fig. 4. Powder bed porosity vs Bond number for all the pharmaceutical powders assuming fixed asperity size of 200 nm for uncoated powers. The Bond numbers were calculated based on (a) median particle size (d_{50}), (b) Sauter mean diameter ($d_{3,2}$), and (c) size class dependent averaging. The solid line is predicted porosity based on Eq. 16, while markers are experimental data

K. Kunnath, L. Chen, K. Zheng et al. Powder Technology 377 (2021) 709–722

number of Eq. 7. The plots display too much scatter, and root mean square error (RMSE) values are fairly high, signifying inadequate prediction. These results do not agree with previous studies which reported very good prediction for powders with a similar range of particle size [9,11]. However, if only the powders common to both the current study as well as Capece et al. [11] were considered, very good prediction can be attained, as is displayed in Fig. 5. The powders used to make Fig. 5 are denoted in Tables 1 and 2 with an asterisk. Although the results of Capece et al. have been validated in Fig. 5, it must be noted that this current study includes much more materials, and attaining similar predictive capability is a lofty goal. Additionally, it appears that the predictive capability is only slightly improved when using the size class dependent Bond number. Although the RSME value in Fig. 4c is lower than the other two plots in Fig. 4, there is still much scatter, and the additional computation required to incorporate size classes does not appear to significantly improve predictive capability.

One key aspect of the plots in Fig. 4 which must be discussed is the effect of dry coating on the powder bed porosity (ε). In these plots, solid markers signify uncoated powders and circle markers signify dry coated powders. Generally, uncoated powders appear to be to the top and/or right of the dry coated powders. This signifies that after dry coating, Bond number approximations and porosity values generally decrease, indicating improved powder bed packing. This aspect has been observed by a previous study [11], hence is also visible in Fig. 5, and is attributed to interparticle cohesion reduction via dry particle coating [25,26]. Additionally, there have been numerous papers which demonstrate the ability of dry coating technique to improve powder properties such as flowability [5,10,12,20,40], dispersibility [16,19,23,25], and deagglomeration [21,35] among other powder properties.

Upon careful inspection of the plots in Fig. 4, it is evident that there are a certain class of powders which cause most of the scatter. They happen to be the same as the outliers in Fig. 2, namely Avicel powders, which are a class of Microcrystalline Cellulose (MCC) excipients produced by FMC Biopolymer. If they are removed from the plots in Fig. 4, it is expected that the scatter would be vastly reduced. As discussed in Section 4.1, Avicel powders have vastly different median particle sizes (20–200 μm), yet they generally have very similar bulk density (ρ_b) and porosity (ε) , as shown in Table 3 and Fig. 2. A notable characteristic for these Avicel powders is that they generally have higher aspects ratios as well as specific surface areas. However, in Table 3, there are several APIs whose powder bed porosities (ε) has been predicted well, both in this study and in previous literature, yet

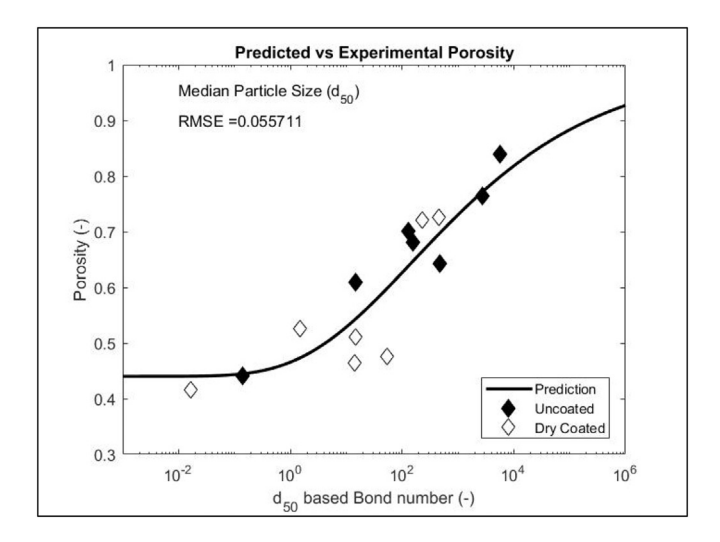


Fig. 5. Powder bed porosity vs Bond number for all the pharmaceutical powders common to this study and Capece et al. [11], which are denoted in Tables 1 and 2 with an asterisk. The Bond numbers were calculated based on median particle sizes, and the solid line represents the predicted porosity based on Eq. 16, while markers are experimental data.

have similarly high aspect ratios [11]. Notice that for these APIs, bulk density (ρ_b) and porosity (ε) vary greatly, depending on particle size (D), which is not the case for the Avicel powders. Thus, powder bed porosity (ε) of Avicel powders is not predicted well, both before and after dry coating. Next, approaches that consider the surface asperities, surface roughness, and surface area to potentially improve powder bed porosity (ε) prediction are discussed.

4.3. Particle surface asperity size corrections

The Bond number calculations discussed in Section 2 have 4 particle scale inputs: particle size (D), particle density (ρ_p) , surface energy (γ_d) , and surface asperity size (d). While the first three inputs are directly measured via laser diffraction (Section 3.2.2), pycnometry (Section 3.2.3) and inverse gas chromatography (Section 3.2.4) respectively, the value for the last input is assumed. Previous work with Bond number models often assume 200 nm as surface asperity size (d), regardless of particle size (D) [9–12,25]. This assumption is based on work by Massimilla and Donsì [33], proven to be adequate for most cases, and accurate porosity prediction (ε) using this estimate was attained in previous literature [9,11,12,25]. However, in light of the poor predictability for porosity results in this study, this assumption needs to be reexamined. Two different approaches will be investigated which may be used to replace the 200 nm surface asperity size (d) assumption.

The first approach uses a proposed empirical relationship that approximates surface asperity size (d) to be proportional to the particle size (D), see Eq. 10 and related details in Section 2 [9,11]. Eq. 10 was used to calculate surface asperity size (d) for all uncoated powders, which are reported in supplementary Table S1, and was subsequently used for Bond number approximations. Fig. 6 displays results of powder bed porosity (ε) , plotted against the surface asperity size (d) adjusted Bond number. Here, only Bond numbers of uncoated particles (solid markers) were approximated using Eq. 10 for surface asperity size (d). For dry coated particle Bond numbers (circle markers), the nano-silica particle size (20 nm) was used as the surface asperity size (d). Visual analysis concludes that there is still much scatter, but RMSE values are slightly lower compared to those reported in Fig. 4. Although surface asperity size (d) approximation of Eq. 10 does slightly improve prediction, it is still does not result in accurate porosity prediction. Notably, most outliers are Avicel powders, both with or without dry coating, which could have been suspected from Fig. 2.

The second approach, although not really predictive, would be to examine if one could back calculate the necessary surface asperity size (d) that would yield perfect prediction, and examine if there is a correlation with some particle scale property. It is emphasized that the purpose behind this exercise is purely for the sake of better understanding the reasons for the deviations in trends from powders such as the Avicels. Accordingly, from experimental porosity (ε) values, the surface asperity size (d) needed for perfect prediction of Avicels and a few selected powders were back-calculated, and are displayed in Table 3 (last column). Very large values of "correct" asperity sizes (d) for Avicels can be observed, and some are even larger than the respective median particle size (d_{50}) and Sauter mean diameter $(d_{3,2})$ for these powders, which is physically impossible. In fact, in order to apply the multi-asperity contact model of Eqs. 3 and 5, the asperity size needs to be one or more orders of magnitude smaller than the host particle size. That means, the d/ D ratio cannot be great than 0.1, and ideally it should be much smaller. Interestingly, such limitation seems to hold for all powders other than Avicels, hence their porosities are predicted well in Fig. 5. Therefore, due to this physical constraint, this attempt to relate correct asperity size (d) to a particle scale property does not work for Avicels.

The results of back-calculated "correct" asperity size (d) are plotted against median particle size (d_{50}) and Sauter mean diameter $(d_{3,2})$ in Fig. 7a and b respectively. In these plots, the dashed line represents 200 nm, which is the surface asperity size (d) assumption used to

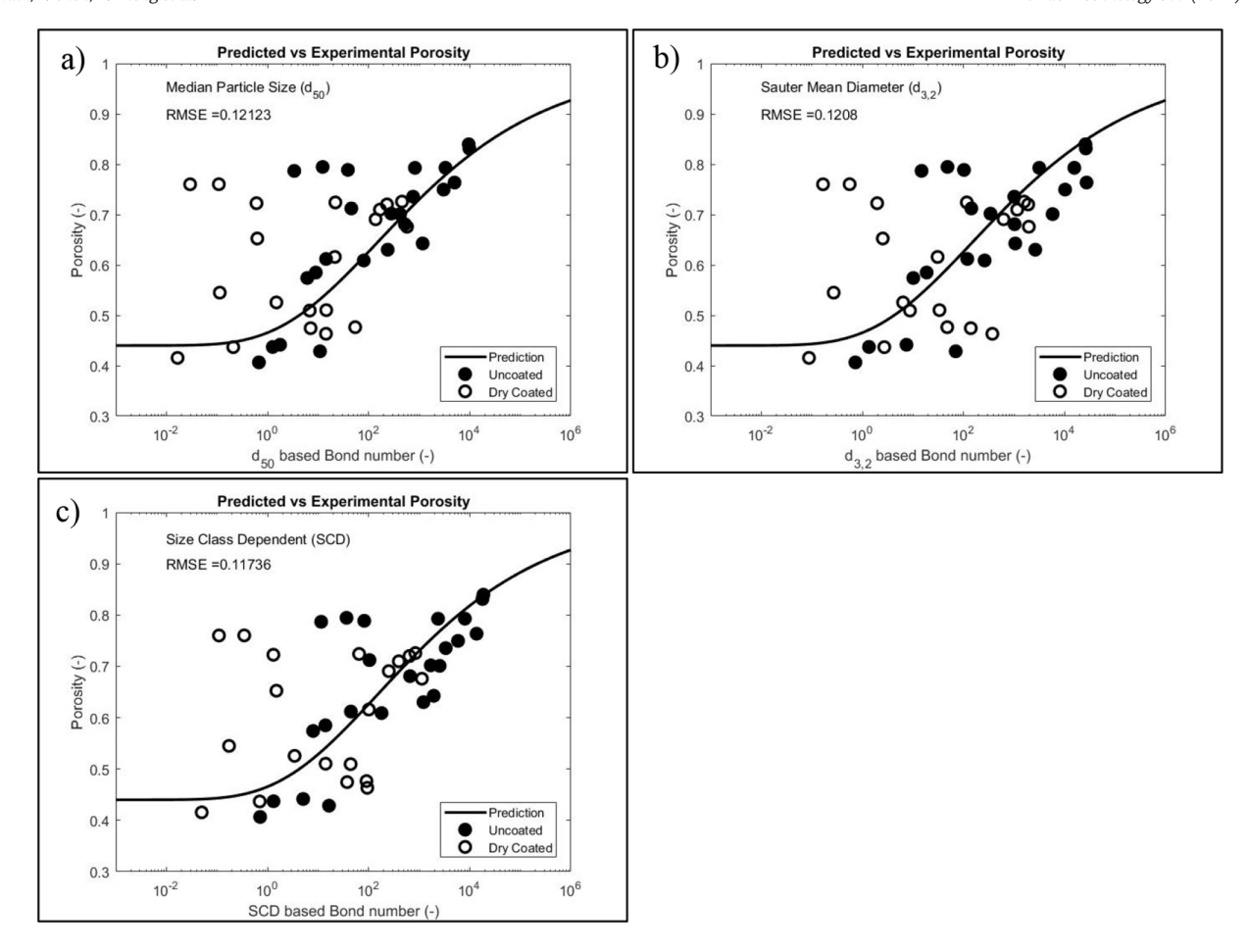


Fig. 6. Powder bed porosity vs Bond number for all pharmaceutical powders when the asperity size is a function of the particle diameter for uncoated powers (Eq. 10). The Bond numbers were calculated based on (a) median particle size (d_{50}), (b) Sauter mean diameter ($d_{3,2}$), and (c) size class dependent averaging. The solid line is predicted porosity based on Eq. 16, while markers are experimental data.

generate the predictions in Fig. 4. The dash-dot line represents the empirical relationship of Eq. 10, which approximates surface asperity size (d) as a fitted power function of particle size (D), and is used to generate the predictions in Fig. 6. For the other powders (solid markers) in these plots, the back-calculated "correct" asperity size (d) can generally be

approximated well by using either the 200 nm assumption (dashed line) or the empirical relationship of Eq. 10 (dash-dot line). However, back-calculated "correct" asperity sizes (d) for Avicels (circle markers) does not seem to be fitted well by either of these. Additionally, the solid lines in Fig. 7a and b are $y = 0.1 \times$, used to represent points

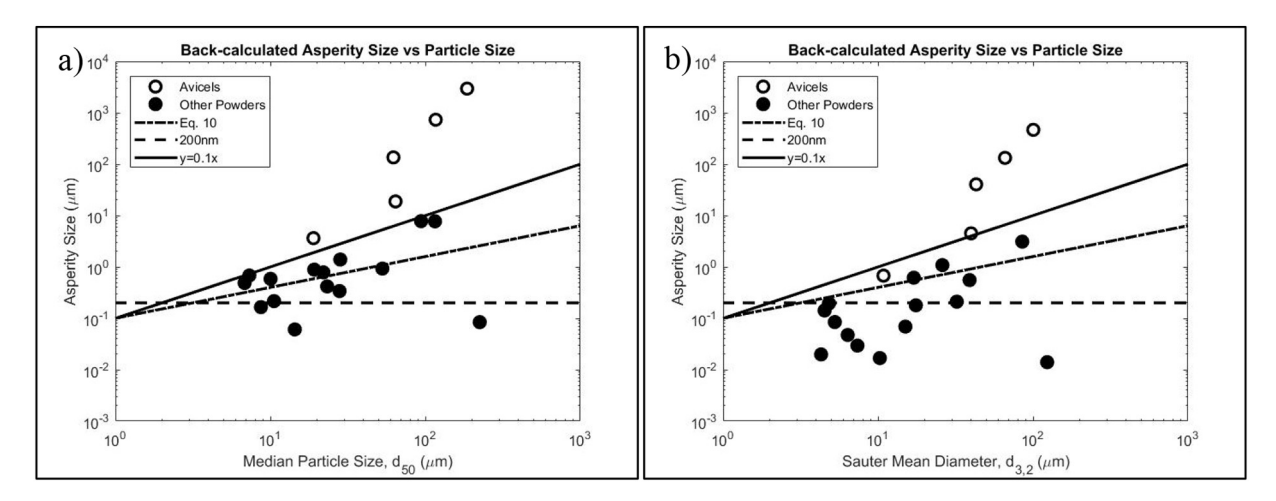


Fig. 7. Back-calculated "correct" asperity sizes that would improve the model fit for Avicels (circle markers) and other powders (solid markers) plotted against (a) median particle size (d_{50}) and (b) Sauter mean diameter ($d_{3,2}$). The horizontal dashed line represents 200 nm, the dash-dot line represents the surface asperity approximation of Eq. 10, and the solid line represents $y = 0.1 \times 10^{10}$. Notice that some Avicels are above the solid line, implying their asperity size is larger than 10% of their particle size, which would violate the multi-asperity model assumptions.

where asperity size (d) is 10% of the particle size (D), which represents the limit of the validity of the multi-asperity model (Egs 3 and 5). Almost all of the Avicel powders are above this line, indicating their "correct" asperity size (d) is invalid being above the model break-down limit. As discussed earlier, this is theoretically incorrect, and surface asperity size (*d*) correction is not possible for Avicel powders. In reality, asperity sizes should be much smaller than particle size, and such is true for the other powders (solid markers). Other approaches to improve powder bed porosity (ε) prediction of Avicels is required. For this, it may be useful to conduct an investigation to elucidate differences between Avicels and other powders whose powder bed porosities (ε) are predicted well by the Bond number model. As a side note, the line representing the model limit, $y = 0.1 \times$, encompasses the Eq. (10) line, indicating that the use of such model that approximates the asperity to be a function of particle size is reasonable, and allows use of the multi-asperity contact model.

4.4. Scanning electron microscopy

Fig. 8 displays Scanning Electron Microscopy (SEM) images of two Avicel (Fig. 8a and b) and two API (Fig. 8c and d) powders. More images of all the Avicels and select other powders are also provided in the supplementary material that have similar trends (Figs. S2 and S3). Additionally, Supplementary Fig. S6 provides SEM images of micronized Acetaminophen before and after dry coating, to illustrate the effect nano-silica dry coating on powder surfaces. From the images in Fig. 8, it is evident that surface morphology of Avicels is much more rough, while others appear to have relatively smooth particle surfaces. Additionally, aspect ratio data is reported in Table 3 for Avicels, and the select APIs whose porosities are predicted well. The aspect ratios of Avicels (Fig. S4) are higher than 1, but appear similar to that of other powders (Fig. S5). These images indicate increased macro-scale surface roughness for Avicels, compared to other powders, and that may be a factor in addition to the effective asperity sizes. Here, the differences in these powders with respect to their size and specific surface area is examined further.

4.5. Surface area analysis

BET adsorption method [41] was used to analyze specific surface area (SSA) of select powders, which are reported in Table 3. Only Avicels and select other powders (APIs), which were used in the previous Bond number based porosity prediction study [11], were selected for BET surface area analysis. While porosity (ε) predictions for Avicels were not good, as discussed before in Section 4.2, the APIs in Table 3 had remarkably good porosity (ε) prediction. It is hoped that any notable differences between these two groups' SSA values may help identify some key characteristic that is different between powders which had adequate porosity (ε) prediction (APIs) and those that did not (Avicels), while having comparable aspect ratios. From the data in Table 3, it is evident that generally, Avicels have much higher SSAs compared to APIs. The only exception is Avicel 301, which has a much lower SSA compared to the rest of the Avicels, yet has a slightly higher SSA than APIs with similar particle size. SSA has an inverse relationship with particle size (D), as displayed in Fig. 9, where SSA values are plotted against Sauter mean diameter $(d_{3,2})$. It is appropriate to use the Sauter mean diameter $(d_{3,2})$ as the x-axis, since it is the representative spherical particle size which has the same surface area to volume ratio as the particles which are measured. In these plots, the solid line represents the theoretical SSA values, calculated using spherical particle assumption. The experimental SSA values of APIs plotted in Fig. 9 (solid markers) indeed have an inverse relationship with particle size, which is expected. Additionally, the APIs' SSA values are similar to the theoretical SSA values of spherical particles (solid line). However, the same could not be said for Avicels. Regardless of size, Avicels (circle markers), including Avicel 301, have higher SSA compared to APIs, and as compared to theoretical SSA values assuming spherical particles, with no clear trend.

From Fig. 9, two conclusions can be made: first is that generally, Avicels have higher SSA values compared to the APIs, indicating Avicels have higher macro-scale surface roughness. The second is that APIs' SSA values are similar to spherical particles, while Avicels have greater deviation from spherical particle nature. Since the particle adhesion models

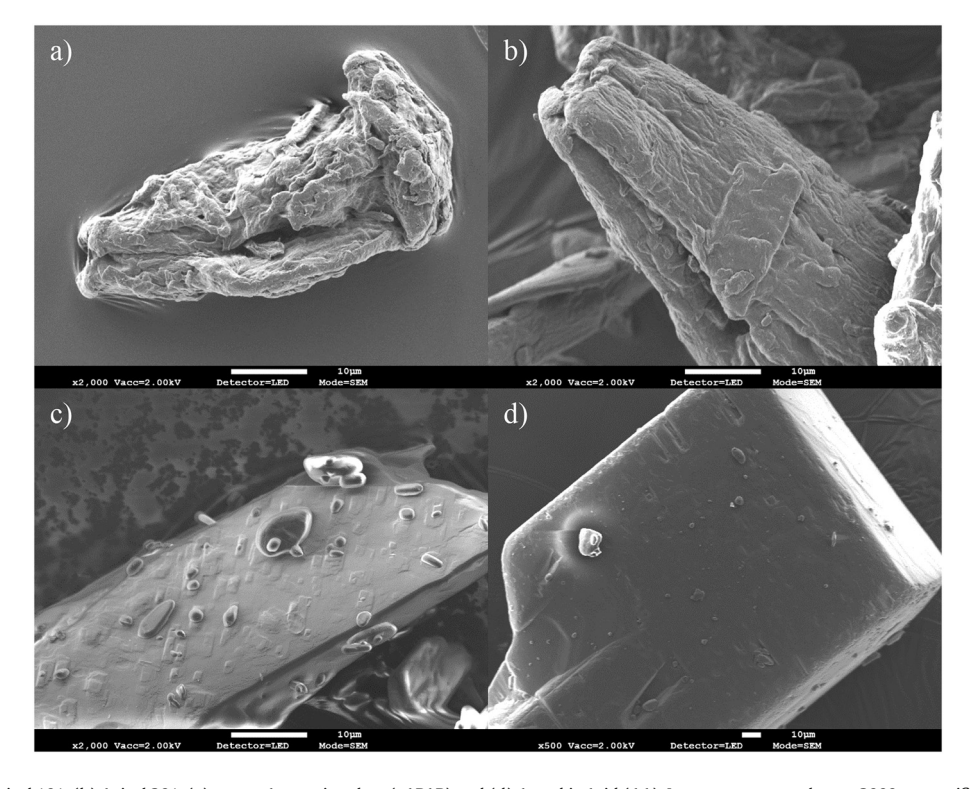


Fig. 8. SEM images of (a) Avicel 101, (b) Avicel 301, (c) coarse Acetaminophen (cAPAP) and (d) Ascorbic Acid (AA). Images a-c were taken at 2000× magnification, while d was taken at 500×. Notice the smoother surface of the particles in c and d, compared to relatively rougher surface of the Avicels (a and b).

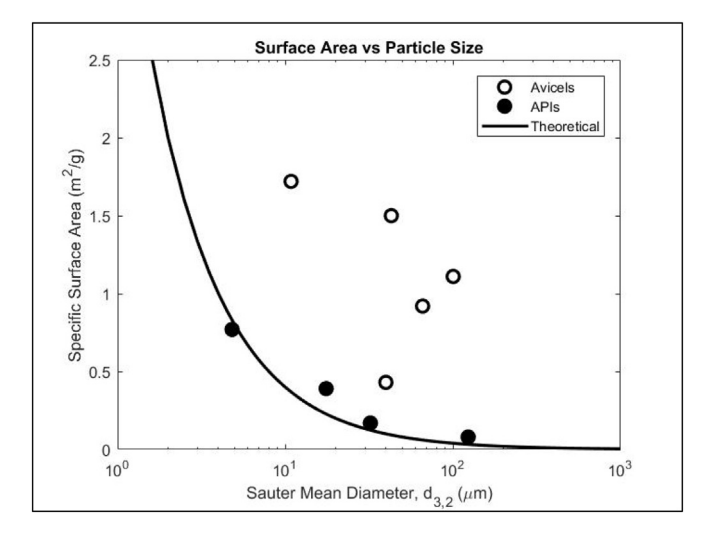


Fig. 9. Experimental specific surface area (SSA) values of all the Avicels (circle markers) and some APIs (solid markers), plotted against Sauter mean diameter $(d_{3,2})$. The solid line represents theoretical SSA, assuming spherical particles with a density of 1500 kg/m³. Notice that Avicels have much higher experimental SSAs compared to APIs, which have experimental SSAs comparable to theoretically calculated values.

needed for the Bond number models assume spherical particles, and in light of these SSA results, it is reasonable that Avicels' powder bed porosity (ε) is not well predicted via Bond number estimation. These results

also possibly explain why the porosity of the API powders can be better predicted. Overall, the examination of the SSA values separate the Avicels from the powders whose porosity prediction is accurate, and may help in rectifying the Bond number estimations in future modeling efforts.

4.6. Model assessment and its applicability

From back-calculated asperity sizes (d) (Section 4.3), SEM images (Section 4.4), and BET surface area results (Section 4.5), it is evident that Avicels are different from other powders and simultaneously have three characteristics that make them unique as compared to other powders. Specifically, they all have high aspect ratios, highly rough surfaces, and high SSAs as compared to equivalent sphere of similar sizes. The multi-asperity model, used to calculate inter-particle vdW force using Eq. 3, assumes relatively smooth spherical particles with densely populated small asperities on the surface. Therefore, it is clear that such model cannot be expected to work well for the Avicels. It would be interesting to see how the model fares if Avicel powders are excluded from Figs. 4 and 6. Fig. 10 displays the powder bed porosity (ε) plotted against Bond number for all powders, excluding Avicels. Surface asperity size (d) was assumed to be 200 nm for uncoated powders, or 20 nm (nano-silica particle size) for dry coated powders. From these plots, it can be observed that experimental data (markers) fit relatively well along the solid line, which represents predicted values. Additionally, the porosity prediction of most new materials used in this study, represented by black markers, is similar to that of powders in common with Capece et al., [11] which are represented by red markers. The trends in

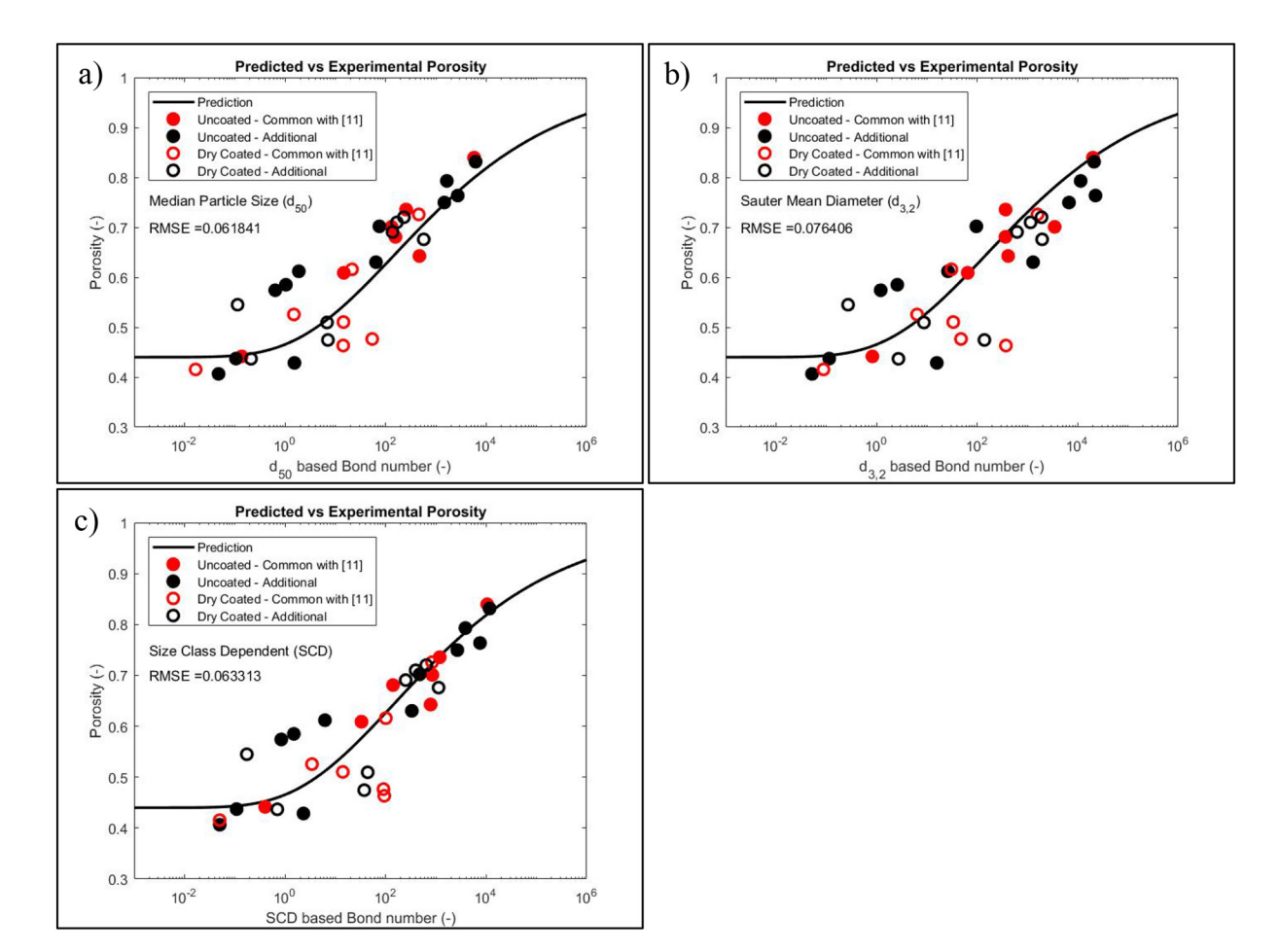


Fig. 10. Powder bed porosity vs Bond number plots for all pharmaceutical powders, except Avicels, which were excluded. The Bond numbers were calculated based on (a) median particle size (d_{50}) , (b) Sauter mean diameter $(d_{3,2})$, and (c) size class dependent averaging. The solid line is predicted porosity based on Eq. 16, while markers are experimental data, with red markers signifying powders in common with Capece et al. [11]. (For interpretation of the references to colour in this figure legend, the reader is referred to the web version of this article.)

Fig. 10 resemble the accurate prediction displayed in Fig. 5, but with a much denser data set. Notice that RMSE values in the Fig. 10 plots are significantly smaller compared to those in Figs. 4 and 6, and closer to the RSME value in Fig. 5, indicating improved predictive capability for the data set without Avicel powders. It can be concluded that for most powders, excluding Avicels, Bond number estimation using the contact model in Eq. 3 provides adequate powder bed porosity (ε) prediction. Interestingly, the model seems to work for certain powders (APIs in Fig. 9 and Table 3) that are not spherical. However, as was discussed in Section 4.5, their deviation from the expected SSA of spherical particles is not large, as seen in Fig. 9, and therefore, they seem to follow the model.

In order to improve predictive capability for the Avicels, the model needs to account for specific characteristics that deviate from its current assumptions. As discussed above, the Avicels have elongated shapes, very rough surfaces, as well as high SSA values as compared to equivalent spherical particles. Since surface roughness and SSA are correlated [42,43], the deviation from the model arises from the combined effect of the particle shape, such as aspect ratio, and the macro-scale surface roughness. To make things more complicated, high-aspect ratio rough particles such as these (Fig. 8a), have pronounced concavities in contrast to the API particles, giving rise to multiple contacts between a pair of contacting particles, higher potential for interlocking, and higher effective friction. All of these lead to poor packing and increased porosity. Addressing all of these effects in the current model is well outside the scope. However, as was demonstrated through DEM simulations, both the higher aspect ratio and higher effective cohesion, which is a result of macro roughness, lead to poorer packing [32]. For example, for particles with aspect ratio of 3 and high cohesion, porosity was very high (>0.7) for a wider range of particle sizes (10–100 μm). These results indicate that the future model improvement needs to address both the effect of particle aspect ratio and effectively high cohesion due to macro roughness or high SSA as compared to equivalent spherical particles. Nonetheless, the current model performs very well considering the wide variations in particle sizes, their size distribution, aspect ratios, material properties including surface energy, and surface modification; major exception being the Avicels that have both macro roughness and non-spherical shape with high SSAs. These results corroborate previous study [11] and confirm that the porosity prediction model had wide applicability.

5. Conclusions

The results demonstrate that the prediction of porosity through the Bond number based model using the cohesion force estimated via multi-asperity contact model [25] works well for many real powders that are cohesive and non-spherical, further corroborating previous results with limited number of non-spherical cases. While that itself is surprising considering the Chen et al. model [25] is valid only for spherical particles, it was equally if not more surprising that the Avicels were outliers, even when some of those were not as cohesive. Upon further investigation, it was discovered that the conventional definition of non-sphericity based on the particle shape aspect ratio alone does not capture the propensity for deviation with the model. In fact, the main factor was an excessive deviation from the specific surface area (SSA) of an equivalent sphere of all the Avicels, which have characteristically different macro roughness and presence of concavity. Compared to all other powders, MCC Avicels had the highest SSA compared to equivalent spheres, while also having high aspect ratios. Addressing such deviations from spherical shape would require extension of the contact models for an improved Bond number prediction. The efforts to improve the porosity prediction through changing the particle size basis for the Bond number prediction did not greatly impact the model's fitting ability. In fact, the model fit was just as good when d50 was used as a basis for the Bond number estimates instead of a more complex approach utilizing the entire particle size distribution. Similarly, better estimates of the natural surface asperity size through an empirical model did not yield appreciable improvement.

For predicting porosity reduction or bulk density enhancement after dry coating, an empirical model was developed so that it may be used by industry practitioners to obtain first order, conservative estimates that justify further investigation. The bulk density enhancement was higher (70–90%) for finer, more cohesive powders, indicating that dry coating works well for the powders for which it is needed the most. Interestingly, even the Avicels followed the predictive model for bulk density improvement after dry coating, which could help improve their functionality compared to other excipients, as reported in recently published work [23,24]. This ability to estimate the expected enhancements after dry coating a priori can guide decision making regarding whether or not dry coating is necessary or would be beneficial.

Nomenclature

Hamaker Constant (I)

Symbols

Α

```
а
           Constant root for Eq. 15(-)
BD_{\Delta Bo}
           Percent increase in bulk density after dry coating (%)
           Percent increase in bulk density after dry coating when
BD_{\Delta 1}
           Bo_g = 1 (\%)
Bo_g
           Bond number (-)
           Size Class Dependent Bond number (-)
Bo_{g,mix}
D
           Particle size of host (m)
D_0
           Cut-off distance (m)
d
           Asperity size (m)
d_{3,2}
           Sauter mean diameter (m)
d_{50}
           Median particle size (m)
           Interparticle van der Waals force (N)
F_{ad}
f_{SA}
           Fractional surface area ( – )
           Gravitational acceleration (m/s<sup>2</sup>)
g
Κ
           Number of size classes (—)
           Distance between two dry coated host particles (m)
L_0
m
           Constant coefficient for Eq. 16 (-)
Ν
           Number of guest particles coated onto one host particle (-)
n
           Constant exponent for Eq. 16(-)
R_c
           Diameter of contact circle (m)
SAC
           Surface area coverage of host particle (—)
W_g
           Weight of host particle (N)
Wt%
           Weight percentage of guest particle (—)
w
           Weighting function (−)
           Equilibrium separation distance (m)
z_0
Greek
           Constant coefficient for Eq. 10(-)
\alpha
β
           Constant exponent for Eq. 10(-)
           Dispersive surface energy (J/m<sup>2</sup>)
\gamma_d
           Powder bed porosity (−)
ε
           Minimum porosity for non-cohesive particles at zero consoli-
\varepsilon_0
           dation(-)
\rho_b
           Bulk density (kg/m<sup>3</sup>)
           Guest particle (true) density (kg/m<sup>3</sup>)
\rho_{g}
           Host particle (true) density (kg/m<sup>3</sup>)
\rho_p
```

Declaration of Competing Interest

Size class index

Size class index

The authors declare that they have no known competing financial interests or personal relationships that could have appeared to influence the work reported in this paper.

Indices

i

j

Acknowledgements

The authors gratefully acknowledge the financial support from the National Science Foundation through grants EEC_0540855 and IIP-1537197, and technical support from Dr. Jeong Seop Shim for BET adsorption experimental assistance. RND is thankful for Fulbright-Nehru Academic and Professional Excellence Senior Research Scholar support.

Appendix A. Supplementary data

Supplementary data to this article can be found online at https://doi.org/10.1016/j.powtec.2020.09.037.

References

- B. van snick, J. Holman, C. Cunningham, A. Kumar, J. Vercruysse, T. De Beer, J. Paul Remon, C. Vervaet, Continuous direct compression as manufacturing platform for sustained release tablets, Int. J. Pharm. 519 (2017) 390–407.
- [2] S.-P. Simonaho, J. Ketolainen, T. Ervasti, M. Toiviainen, O. Korhonen, Continuous manufacturing of tablets with PROMIS-line — introduction and case studies from continuous feeding, blending and tableting, Eur. J. Pharm. Sci. 90 (2016) 38–46.
- [3] L.X. Yu, G. Amidon, M.A. Khan, S.W. Hoag, J. Polli, G.K. Raju, J. Woodcock, Understanding pharmaceutical quality by design, AAPS J. 16 (2014) 771–783.
- [4] L.X. Yu, Pharmaceutical quality by design: product and process development, understanding, and control, Pharm. Res. 25 (2008) 781–791.
- [5] Z. Huang, J.V. Scicolone, X. Han, R.N. Davé, Improved blend and tablet properties of fine pharmaceutical powders via dry particle coating, Int. J. Pharm. 478 (2015) 447-455
- [6] R. Yang, R.P. Zou, A. Yu, Computer simulation of packing of fine particles, Phys Rev E Stat Phys Plasmas Fluids Relat Interdiscip Topics 62 (2000) 3900–3908.
- [7] E.C. Abdullah, D. Geldart, The use of bulk density measurements as flowability indicators, Powder Technol. 102 (1999) 151–165.
- [8] C.C. Sun, Setting the bar for powder flow properties in successful high speed tableting, Powder Technol. 201 (2010) 106–108.
- [9] A.B. Yu, C.L. Feng, R.P. Zou, R.Y. Yang, On the relationship between porosity and interparticle forces, Powder Technol. 130 (2003) 70–76.
- [10] M. Capece, R. Ho, J. Strong, P. Gao, Prediction of powder flow performance using a multi-component granular bond number, Powder Technol. 286 (2015) 561–571.
- [11] M. Capece, Z. Huang, D. To, M. Aloia, C. Muchira, R.N. Davé, A.B. Yu, Prediction of porosity from particle scale interactions: surface modification of fine cohesive powders, Powder Technol. 254 (2014) 103–113.
- [12] M. Capece, K.R. Silva, D. Sunkara, J. Strong, P. Gao, On the relationship of interparticle cohesiveness and bulk powder behavior: flowability of pharmaceutical powders, Int. J. Pharm. 511 (2016) 178–189.
- [13] B. Van Snick, J. Dhondt, K. Pandelaere, J. Bertels, R. Mertens, D. Klingeleers, G. Di Pretoro, J.P. Remon, C. Vervaet, T. De Beer, V. Vanhoorne, A multivariate raw material property database to facilitate drug product development and enable in-silico design of pharmaceutical dry powder processes, Int. J. Pharm. 549 (2018) 415–435.
- [14] M. Capece, Z. Huang, R. Davé, Insight into a novel strategy for the design of tablet formulations intended for direct compression, J. Pharm. Sci. 106 (2017) 1608–1617.
- [15] C. Ghoroi, L. Gurumurthy, D.J. McDaniel, L.J. Jallo, R.N. Davé, Multi-faceted characterization of pharmaceutical powders to discern the influence of surface modification, Powder Technol. 236 (2013) 63–74.
- [16] C. Ghoroi, X. Han, D. To, L. Jallo, L. Gurumurthy, R.N. Davé, Dispersion of fine and ultrafine powders through surface modification and rapid expansion, Chem. Eng. Sci. 85 (2013) 11–24.
- [17] X. Han, C. Ghoroi, R. Davé, Dry coating of micronized API powders for improved dissolution of directly compacted tablets with high drug loading, Int. J. Pharm. 442 (2013) 74–85

- [18] X. Han, C. Ghoroi, D. To, Y. Chen, R. Davé, Simultaneous micronization and surface modification for improvement of flow and dissolution of drug particles, Int. J. Pharm. 415 (2011) 185–195.
- [19] X. Han, L. Jallo, D. To, C. Ghoroi, R. Davé, Passivation of high-surface-energy sites of milled ibuprofen crystals via dry coating for reduced cohesion and improved flowability, J. Pharm. Sci. 102 (2013) 2282–2296.
- [20] Z. Huang, J.V. Scicolone, L. Gurumuthy, R.N. Davé, Flow and bulk density enhancements of pharmaceutical powders using a conical screen mill: a continuous dry coating device, Chem. Eng. Sci. 125 (2015) 209–224.
- [21] Z. Huang, W. Xiong, K. Kunnath, S. Bhaumik, R.N. Davé, Improving blend content uniformity via dry particle coating of micronized drug powders, Eur. J. Pharm. Sci. 104 (2017) 344–355.
- [22] LJ. Jallo, C. Ghoroi, L. Gurumurthy, U. Patel, R.N. Davé, Improvement of flow and bulk density of pharmaceutical powders using surface modification, Int. J. Pharm. 423 (2012) 213–225.
- [23] L. Chen, X. Ding, Z. He, S. Fan, K.T. Kunnath, K. Zheng, R.N. Davé, Surface engineered excipients: II. Simultaneous milling and dry coating for preparation of fine-grade microcrystalline cellulose with enhanced properties, Int. J. Pharm. 546 (2018) 125–136.
- [24] L. Chen, X. Ding, Z. He, Z. Huang, K.T. Kunnath, K. Zheng, R.N. Davé, Surface engineered excipients: I. Improved functional properties of fine grade microcrystalline cellulose, Int. J. Pharm. 536 (2018) 127–137.
- [25] Y. Chen, J. Yang, R.N. Dave, R. Pfeffer, Fluidization of coated group C powders, AICHE J. 54 (2008) 104–121.
- [26] J. Yang, A. Sliva, A. Banerjee, R.N. Dave, R. Pfeffer, Dry particle coating for improving the flowability of cohesive powders, Powder Technol. 158 (2005) 21–33.
- [27] R.M. German, Particle Packing Characteristics, 1989.
- [28] A.B. Yu, R.P. Zou, N. Standish, Modifying the linear packing model for predicting the porosity of nonspherical particle mixtures, Ind. Eng. Chem. Res. 35 (1996) 3730–3741.
- [29] A.-B. Yu, N. Standish, A. McLean, Porosity calculation of binary mixtures of nonspherical particles, J. Am. Ceram. Soc. 76 (1993) 2813–2816.
- [30] S.T. Nase, W.L. Vargas, A.A. Abatan, J.J. McCarthy, Discrete characterization tools for cohesive granular material, Powder Technol. 116 (2001) 214–223.
- [31] A.C. Hoffmann, H.J. Finkers, A relation for the void fraction of randomly packed particle beds, Powder Technol. 82 (1995) 197–203.
- [32] X.L. Deng, R.N. Davé, Dynamic simulation of particle packing influenced by size, aspect ratio and surface energy, Granul. Matter 15 (2013) 401–415.
- [33] L. Massimilla, G. Donsi, Cohesive forces between particles of fluid-bed catalysts, Powder Technol. 15 (1976) 253–260.
- [34] J.N. Israelachvili, 6 Van der Waals Forces, Intermolecular and Surface Forces, (Third Edition) Academic Press, San Diego, 2011 107–132.
- [35] A. Castellanos, The relationship between attractive interparticle forces and bulk behaviour in dry and uncharged fine powders, Adv. Phys. 54 (2005) 263–276.
- [36] Y. Chen, M.A.S. Quintanilla, J. Yang, J.M. Valverde, R.N. Dave, Pull-off co f coated
- fine powders under small consolidation, Phys. Rev. E 79 (2009), 041305.
 [37] A.B. Yu, J. Bridgwater, A. Burbidge, On the modelling of the packing of fine particles, Powder Technol. 92 (1997) 185–194.
- [38] J. Schultz, L. Lavielle, C. Martin, The role of the interface in carbon fibre-epoxy composites, J. Adhes. 23 (1987) 45–60.
- [39] K. Sing, The use of nitrogen adsorption for the characterisation of porous materials, Colloids Surf. A Physicochem. Eng. Asp. 187-188 (2001) 3-9.
- 40] K. Kunnath, Z. Huang, L. Chen, K. Zheng, R. Davé, Improved properties of fine active pharmaceutical ingredient powder blends and tablets at high drug loading via dry particle coating, Int. J. Pharm. 543 (2018) 288–299.
- [41] S. Brunauer, P.H. Emmett, E. Teller, Adsorption of gases in multimolecular layers, J. Am. Chem. Soc. 60 (1938) 309–319.
- [42] M. Rahimi, F. Dehghani, B. Rezai, M.R. Aslani, Influence of the roughness and shape of quartz particles on their flotation kinetics, Int. J. Miner. Metall. Mater. 19 (2012) 284–289.
- [43] Z. Li, F. Rao, M.A. Corona-Arroyo, A. Bedolla-Jacuinde, S. Song, Comminution effect on surface roughness and flotation behavior of malachite particles, Miner. Eng. 132 (2019) 1–7.